

Communication

Wavelength Effects on the Reflectivity of Niobium by Solid-State Laser Pulses

Olena Benavides ^{1,*} , Lelio de la Cruz May ¹ , Aaron Flores Gil ¹ and Efrain Mejia Beltran ² ¹ Facultad de Ingeniería, Universidad Autónoma del Carmen, Cd. del Carmen C.P. 24180, Campeche, Mexico² Centro de Investigaciones en Óptica, León C.P. 37150, Guanajuato, Mexico

* Correspondence: obenavides@pampano.unacar.mx

Abstract: This study utilized solid-state lasers with a 50 ns pulse duration in a Q-switched mode of operation at wavelengths of 1.06 μm and 0.69 μm to investigate the hemispherical reflectivity of niobium. Our experimental results show that the reflectivity of niobium decreases notably as the laser fluence increases towards the plasma formation threshold for ablation at both studied wavelengths, which we attribute to changes in the absorptivity of the surface resulting from plasma formation. We also observed a significant effect of laser wavelength on the reflectivity values of the sample at low laser fluence. By determining the threshold fluence values for each wavelength, we estimated the surface temperature associated with the threshold fluence for plasma formation. Our calculations revealed discrepancies between published values for optically polished and mechanically polished niobium, which we suggest may be due to the presence of nano/micro defects, oxide films, and contaminants that amplify the wavelength-dependent effects on reflectivity. These findings have important implications for the design of optical components and laser processing techniques that use niobium, as well as for the development of accurate models of laser-material interactions. Further research is needed to fully understand the underlying mechanisms driving the observed effects and to explore potential applications of niobium in laser-based technologies.

Keywords: laser ablation; damage threshold; reflectivity; laser wavelength effect; metals



Citation: Benavides, O.; de la Cruz May, L.; Flores Gil, A.; Mejia Beltran, E. Wavelength Effects on the Reflectivity of Niobium by Solid-State Laser Pulses. *Photonics* **2023**, *10*, 402. <https://doi.org/10.3390/photonics10040402>

Received: 9 February 2023

Revised: 14 March 2023

Accepted: 27 March 2023

Published: 3 April 2023



Copyright: © 2023 by the authors. Licensee MDPI, Basel, Switzerland. This article is an open access article distributed under the terms and conditions of the Creative Commons Attribution (CC BY) license (<https://creativecommons.org/licenses/by/4.0/>).

1. Introduction

Nanosecond laser ablation of solids is used in numerous applications such as self-folding metals [1], thin film deposition [2,3], nano/micro laser-processing of materials [4–8], 3D printing of common metals by laser-induced forward transfer [9], parameterization of optical properties [10,11], fractionation [12], laser-induced breakdown spectroscopy [13], design of hydrophobic materials [14,15], microfluidics [16], and others. Although many studies have investigated high-intensity nanosecond pulsed laser ablation, the effect of wavelength on the reflectivity of metals is still being investigated. Bonch-Bruevich et al. [17] were the first to study the reflectivity of metals irradiated by high-intensity laser pulses and found a substantial drop in total reflectivity experimentally. Basov et al. [18] studied the total reflectivity of Cu, Sn, and Al when irradiated by 15-ns Nd-laser pulses, varying laser fluence from 3×10^7 to 3×10^{10} W/cm². Results show a sharp decrease of reflectivity values for ablation in a vacuum. Previous experiments [19–21] studying the reflectivity of metals by laser pulses in the ablation regime exhibited the same reduction of reflectivity associated with plasma formation on the surface of the sample.

Our research was conducted on niobium, a metal of great interest in the technology industry [22]. Niobium is used to strengthen alloys, especially at low temperatures [23]. Alloys containing niobium are used in jet engines and rockets, girders for buildings and oil platforms, oil and gas pipelines, and superconductor wires for superconductor magnets [24]. However, previous studies have only focused on the effect of laser fluence on the reflectivity of the sample [20,21]. Therefore, the aim of this study is to investigate the effect of laser

wavelength on the total hemispherical reflectivity of niobium in ablation by nanosecond Nd: YAG laser pulses in air at atmospheric pressure. Reflectivity is a crucial factor in laser ablation, as it determines how much laser energy is absorbed or reflected by the material being targeted [25]. High reflectivity can result in inefficient ablation, while low reflectivity can lead to more efficient ablation. Understanding the reflectivity of the target material, especially for metals, is vital, as it depends on various factors, including the wavelength of the incident light [26,27]. Reflectivity can affect the depth of ablation, and surface plasmon resonances can impact reflectivity at specific wavelengths [28]. Therefore, investigating the dependence of reflectivity on wavelength is crucial to optimize laser ablation for different applications [29–33]. We used two laser wavelengths ($\lambda_1 = 1.06$ and $\lambda_2 = 0.69$ μm) to investigate the effect of wavelength on sample reflectivity.

The hemispherical total reflection was studied as a function of laser fluence in the range of 0.1–100 J/cm². All samples were mechanically polished with a 0.3- μm -grade aluminum oxide powder. For our research, we used bulk niobium with 96% purity as the material of interest. The samples had a thickness of 1.5 mm, but the surfaces were not ideal and may have contained initial surface impurities, oxides, adsorbates, and structural defects, as is often the case in practical materials processing. Initial conditions were the same for each experiment. Initial conditions are the same for each experiment.

2. Materials and Methods

Figure 1 shows the experimental setup used to investigate laser light reflection in ablation. Two types of lasers with different wavelengths, an Nd: YAG laser with $\lambda_1 = 1.06$ μm and a ruby laser with $\lambda_2 = 0.69$ μm , were used to investigate a wider range of phenomena and gain a more comprehensive understanding of the reflectivity of niobium. The pulse duration of both lasers was approximately 50 ns at FWHM, and the laser fluence was controlled by a calibrated variable attenuator.

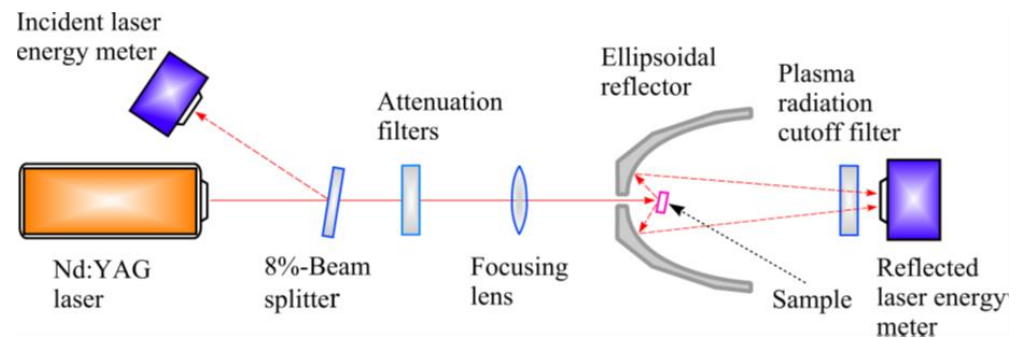


Figure 1. Experimental setup to study the reflection of laser light in niobium ablation.

To study reflection, we focus the laser beam onto a mechanically polished bulk niobium sample using a lens with a focal length of 250 mm. We employ a technique that uses a hemiellipsoidal light reflector to collect both specular and diffuse components of the reflected light. Collecting both components is important because the laser pulse damages the sample surface, which can cause scattering of the reflected light. The sample is placed in the internal focal point of the hemiellipsoidal reflector and tilted at a 19-degree angle relative to the laser beam axis to reduce laser light backscattering through the entrance hole in the reflector. We measure the energy of the laser pulse reflected by the sample using a joulemeter placed in the external focal point of the reflector. To measure the energy of the laser pulse incident onto the sample, we use a beam-splitter to direct a fraction of the laser beam onto another joulemeter (as shown in Figure 1). We calculate the hemispherical total reflectivity, R (a sum of specular and diffuse components of the reflected light) as $R = E_{refl} / E_{inc}$, where E_{refl} is the energy of the reflected laser pulse and E_{inc} is the energy of the incident laser pulse. The incident laser fluence, F , is determined by dividing the

incident laser pulse energy, E_{inc} , by the laser spot area on the sample. We study the total reflectivity in a laser fluence range of 0.06–100 J/cm².

All experiments were conducted at atmospheric pressure. The sample was moved using a computer-controlled X-Y translator to target a new area of the surface with each laser pulse. The surface damage and plasma formation thresholds were measured. The damage threshold was defined as the minimum single-pulse fluence at which visible surface damage was observed under an optical microscope. The plasma formation threshold was determined using a technique proposed by [25], which involved detecting a bright violet flash at the irradiated point. The flash was detected using a photomultiplier with a 0.45 μm long-wavelength cutoff filter with transmittance less than 0.9% and an optical density of 2.5. A cutoff filter was used to prevent plasma radiation from entering the energy meter.

The niobium sample was prepared in the form of a mechanically polished plate with a thickness of 1.5 mm and dimensions of 2×2 cm. Although it is preferable to have samples with optically flat surfaces, achieving this requires specific, often expensive processes. To ensure accurate measurements of laser reflectivity, the measuring setup was calibrated using mechanically polished metal samples at low laser fluence. The calibration samples were measured using a Perkin-Elmer Lambda 900 spectrophotometer with an integrating sphere. It should be noted that the ellipsoidal reflector used in the setup absorbs a small amount of the laser light reflected from the sample, and there are also losses due to the chamber rear window and plasma radiation cutoff filter. By calibrating the setup at low laser fluence, the effects of these losses were minimized, allowing for more accurate measurements of laser reflectivity.

A scanning electron microscope was used to characterize the defects in the structural surface of the mechanically polished samples [34,35]. The obtained images show micro- and nano-defects present on the surface of bulk metal samples.

Figure 2 shows the total reflectivity of niobium as a function of laser fluence at atmospheric pressure for both wavelengths. Note that the reflectivity values for $\lambda_1 = 1.06 \mu\text{m}$ are higher than those for $\lambda_2 = 0.69 \mu\text{m}$. At low laser fluences, the reflectivity values remain constant at 0.75 and 0.68, respectively, and the irradiated surface does not undergo any surface damage until the fluence reaches the plasma ignition threshold. In this study, we determined the plasma formation thresholds to be 2 J/cm² and 1.3 J/cm², respectively, based on an average of ten measurements. We also found that the damage threshold values were only slightly lower than the plasma formation fluence values, at 1.7 J/cm² and 1.2 J/cm² for wavelengths 1.06 μm and 0.69 μm , respectively.

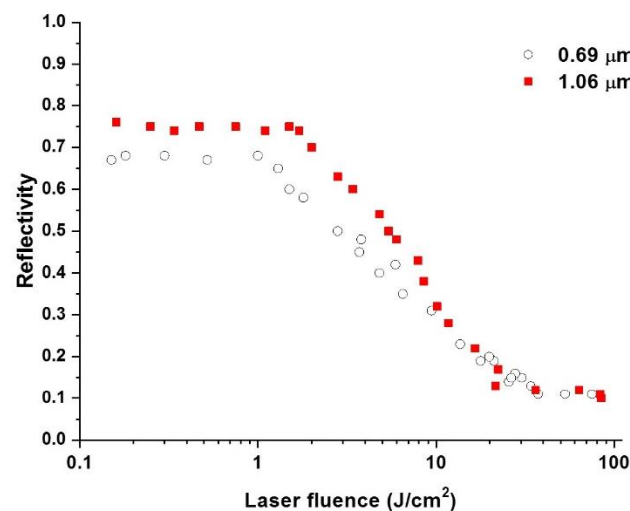


Figure 2. Experimental reflectivity values for bulk niobium when irradiated by laser wavelengths $\lambda = 1.06$ and $0.69 \mu\text{m}$ in air at atmospheric pressure.

Figure 2 also shows the effect of laser wavelength on the reflectivity of the material. Note that the reflectivity values are very different for each laser wavelength. As the laser fluence increases further, the reflectivity drops to about 0.1 for both wavelengths, and the effect of laser wavelength becomes insignificant since the reflectivity values remain unchanged with further increases in laser fluence. This drop in reflectivity with increasing laser power is attributed to plasmonic absorption, which refers to the phenomenon in which plasma (a highly ionized gas) absorbs electromagnetic radiation in the radio frequency range. Vorobyev and Guo [36] suggest that this phenomenon plays a more important role in reducing the reflectivity with increasing laser power. The experimental results suggest that the plasma formed by the shorter-wavelength laser ($\lambda = 0.69 \mu\text{m}$) absorbs more laser energy than the plasma formed by the longer-wavelength laser ($\lambda = 1.06 \mu\text{m}$), which results in a greater reduction in reflectivity at higher laser fluences for the shorter wavelength. This difference in plasma behavior may be due to differences in the absorption and ionization properties of the material at different wavelengths. We assume that this fact plays an important role in reducing the wavelength effect on the total reflection at $F > 10 \text{ J/cm}^2$ in our experimental data shown in Figure 2.

3. Discussion

Note that for the longer wavelength ($1.06 \mu\text{m}$), reflectivity values drop earlier than they do for $\lambda = 0.69 \mu\text{m}$. This could be due to shorter wavelengths being absorbed more efficiently by metals than longer ones [37]. This agrees with the fact that plasma formation occurs at a lower laser fluence for $\lambda = 0.69 \mu\text{m}$ than for $\lambda = 1.06 \mu\text{m}$.

Reflectivity reduction can be caused by the temperature dependence of the optical constants [38–40] and the absorption of laser light by laser-induced plasma [18,19]. In order to explain the role of the temperature dependence of the optical constants on the reflectivity, the surface temperatures of the samples at the plasma formation threshold fluences have been computed using Drude’s equation derived by Reedy [41] (Figure 3).

$$T_{\text{surf}}(t) = \frac{(1 - R)\sqrt{a}}{k\sqrt{\pi}} \int_0^t \frac{I(t - \tau)}{\sqrt{\tau}} d\tau + T_0 \quad (1)$$

where a is the thermal diffusivity, k is the thermal conductivity, I is the radiation intensity of the incident laser beam in function of time, t and the integration variable τ , T_0 is the initial temperature. The surface temperature equation is calculated for each wavelength using the following parameters: For $\lambda_1 = 1.06 \mu\text{m}$, $k = 53.7 \text{ W/(m}\cdot\text{K)}$, $a = 2.321 \times 10^{-5} \text{ m}^2/\text{s}$, $T_0 = 20 \text{ }^\circ\text{C}$, $R = 0.75$, and for $\lambda_2 = 0.69 \mu\text{m}$ $R = 0.68$, and are shown in Figure 3. Note that the maximum surface temperatures are $1945 \text{ }^\circ\text{C}$ and $1618 \text{ }^\circ\text{C}$ for wavelengths λ_1 and λ_2 , respectively.

The computed maximum surface temperatures calculated at the plasma formation threshold fluences are significantly smaller than the melting point of the studied metal ($2477 \text{ }^\circ\text{C}$).

The reflectivity data shows that the reflectivity values of the studied samples do not change at least up to the plasma formation threshold. Classical Drude free-electron theory predicts a decrease in reflectivity with an increase in temperature [42]. For near-infrared, the temperature dependence of the Drude reflectivity of metals is given by the following approximation [40]:

$$R(T) \approx 1 - \frac{\omega_p}{2\pi\sigma_0(T)} \quad (2)$$

where T is the temperature, σ_0 is the DC electric conductivity, $\omega_p = \left(\frac{4\pi n_e e^2}{m_e}\right)^{\frac{1}{2}}$ is the electron plasma frequency in the metal, n_e is the density of free electrons in the metal, e is the charge of the electron, and m_e is the effective electron mass. The Drude theory only applies to metal surfaces that are ideally smooth and clean. Surfaces close to ideal ones can be only produced by the deposition of thin films under ultra-high vacuum conditions. It has been previously stated that real metal surfaces are commonly oxidized,

contaminated, covered with adsorbates, and have structural defects that can enhance absorptivity $A = (1 - R)$. Therefore, the absorptivity for a real smooth surface is given by [43].

$$A = (1 - R) = A_{IN} + A_{IM} + A_{OX} + A_{AD} + A_{SD} \quad (3)$$

where A_{IN} , is the intrinsic absorptance of the ideal surface given by the Drude theory, and A_{IM} , A_{OX} , A_{AD} , and A_{SD} are contributions from surface impurities, oxides, adsorbates, and surface structural defects, respectively. These contributions can be temperature dependent, causing the resulting temperature dependence of A or R to be different from that predicted by the Drude theory. Since the obtained data shows that the reflectivity does not change from room temperature up to the plasma formation threshold, where reflectivity begins to decrease, we assume that the sharp drop in reflectivity values is caused by a plasma shielding effect.

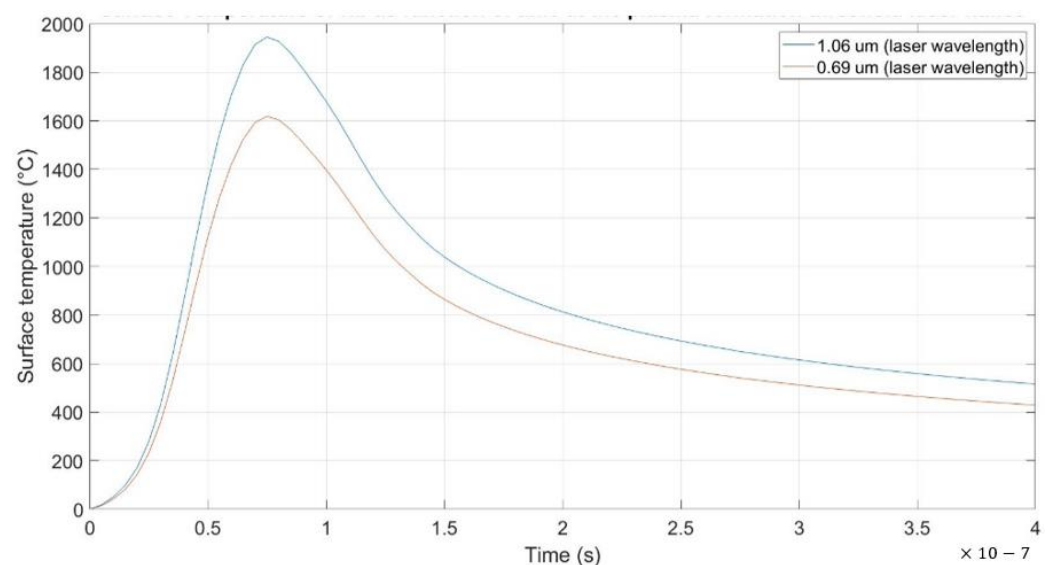


Figure 3. Computed surface temperature of the Nb samples as a function of time at the plasma formation threshold laser fluence.

Hence, the reflectivity drops occurring in our experiment at 1945 °C and 1618 °C cannot be explained by the temperature dependence of the optical properties. This suggests that the micro- and nano-defects on the surface of the sample play an important role in the early optical breakdown of the sample. Surface heating by laser radiation of various microstructural defects by nanosecond laser pulses and its effects on plasma formation on bulk aluminum in air has been previously studied [44]. The authors found that lamination and pit-type defects are the most common potential initiation sites on practical metal surfaces. Moreover, they showed that these defects are heated more rapidly to a significantly higher temperature than bulk aluminum surface.

In a previous experimental study [45], the absorptivity of bulk metal targets irradiated by giant ruby laser pulses was measured using micro craters. The metals studied were Cu, Al, Mg, Cd, and Sn. The author found that during the initial stage of advanced evaporation, absorption of laser radiation occurs mainly in pit-type defects, or micro-craters, on the metal surfaces. The depth of the craters on the investigated metal targets was approximately 5–10 μm. Abrupt changes in the absorptivity of the metals were attributed to optical breakdown on the target surface.

Therefore, the discrepancy between the experimental results and the theoretical predictions can be explained by the fact that the theoretical calculation is only valid for ideally polished and clean metal surfaces. For practical surfaces, which are commonly contaminated, oxidized, covered with adsorbents, and have nano/microstructural defects, Drude's theorem may not be applicable as explained in [46].

We attribute the sharp decrease in reflectivity values to the plasma absorption effect since the onset of the decrease occurs at a laser fluence only slightly above the damage threshold and correlates with the plasma ignition threshold. The reflection of the laser light under conditions of plasma generation has already been widely discussed in [19] and later in [36]. Figure 4 shows the reflection process in this case. Two types of laser-induced plasmas for ablation in air have been defined, material-ablated plasma, and ambient gas plasma. Additionally, ambient gas plasma can take the form of a laser-supported combustion wave or a detonation wave, depending on the laser fluence intensity [47,48].

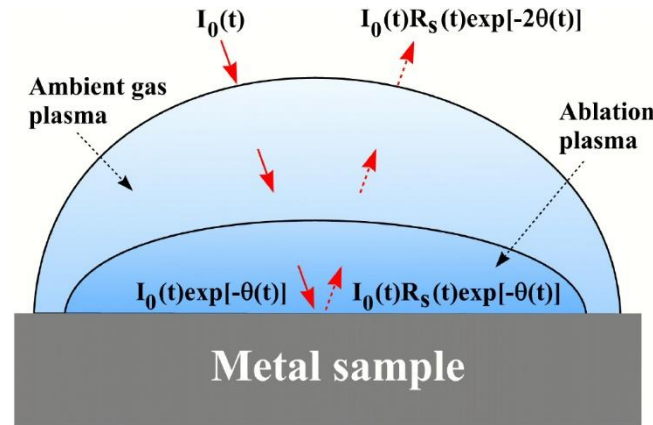


Figure 4. Schematics of laser-induced plasmas and reflection of the laser pulse from the sample-plasma system, where $I_0(t)$ is the incident laser pulse power, $I_0(t) \exp[-\theta(t)]$ is the laser pulse power that arrives at the sample surface, $\theta(t)$ is the total optical thickness of the plasma, $I_0(t) R_s(t) \exp[-\theta(t)]$ is the laser pulse power reflected from the sample surface, $R_s(t)$ is the reflectivity of the sample surface, and $I_0(t) R_s(t) \exp[-2\theta(t)]$ is the laser pulse power that escapes the sample-plasma system.

Considering the absorption of the laser beam in the plasma, the time-integrated reflectivity is given by [19].

$$R = \frac{(\int_0^{\tau_L} I_0(t) R_s(t) \exp[-2\theta(t)] dt)}{\int_0^{\tau_L} I_0(t) dt} \tag{4}$$

where $I_0(t)$ is the pulse power of the incident laser in function of time, $R_s(t)$ is the reflectivity of the sample surface, $\theta(t)$ is the total optical thickness of the plasma, and τ_L is the duration of the laser pulse. Equation (4) shows that R depends on both the total optical thickness of the plasma θ and the reflectivity of the surface R_s .

In general, the total wavelength effect on the light reflection in the ablation depends on both the laser light absorption in the surface layer of the sample and in the plasma. The reflectivity wavelength dependence on the surface layer is described by the Fresnel and Drude formulae [49]. For a smooth, flat, and clean surface, the reflectivity is given by:

$$R = \left| \frac{\epsilon^{\frac{1}{2}} - 1}{\epsilon^{\frac{1}{2}} + 1} \right|^2 = \frac{(n - 1)^2 + k^2}{(n + 1)^2 + k^2} \tag{5}$$

where ϵ is the complex dielectric function, n is the refractive index, and k is the extinction coefficient. For metals, ϵ is given by the relation [47,48].

$$\epsilon(\omega) = 1 - \frac{\omega_p^2}{\omega(\omega - i\nu_{eff})} \tag{6}$$

where ω is the angular frequency of the laser light, $\nu_{eff} = \nu_{e-ph} + \nu_{e-e}$ is the effective collision frequency, and ν_{e-ph} and ν_{e-e} are the contributions of electron-phonon and

electron–electron collisions, respectively. In contrast to femtosecond laser pulses [50], the contribution of v_{e-e} is small in the case of nanosecond laser pulses. Equations (5) and (6) predict an increase in reflectivity with the increase in light wavelength. In this case, the energy per photon is 1.17 and 1.8 eV for 1.06 μm and 0.69 μm , respectively.

Using the values in the table of n and k for niobium [51], Equation (5) gives $R = 0.82$ and $R = 0.60$ for 1.06 μm and 0.69 μm , respectively. These calculated reflectivity values differ from those measured in this study ($R = 0.75$ for $\lambda = 1.06 \mu\text{m}$, and $R = 0.68$ for $\lambda = 0.69 \mu\text{m}$). However, they are in good agreement with the reflectivity values shown in [52].

The discrepancies between our reflectivity values and the calculated values shown are explained by the fact that the n and k table values were obtained for a thin, clean, and smooth film of high optical quality and purity (99.9% niobium) [53]. However, in most practical applications the actual sample surface is not ideal and has nano/microstructural defects, an oxide layer, and pollutants, which result in different reflectivity values, such as in our case.

Very little is known about the reflectivity of a surface that undergoes ablation and is screened by plasma (terms $R_s(t)$ in Equation (4)). Ablation has shown to be dominantly driven by vaporization and phase explosion mechanisms, depending on the laser fluence [6,54,55]. The phase explosion threshold for metals is in the range of 3.9–15 J/cm^2 [51,56,57]. In higher fluences, such as in our case, solid sample surfaces become liquid and can be further changed into a supercritical fluid state. In the literature [57–59], there are several examples of studies conducted on the optical properties of liquid metals. It has been demonstrated that the reflection of light by liquid metals is well described by the Fresnel and Drude equations. However, the main limitation when it comes to modeling reflection from liquid layers produced in laser ablation is to take into account transient geometrical fluctuations of the surface profile caused during the laser pulsed ablation. For example, nanoscale transient ripples on the surface of the melted layer can affect reflectivity through the Fresnel angular dependence.

To our knowledge, optical properties of transient nano/micro ripples induced on a metal surface by a nanosecond laser pulse remain unstudied.

The phase explosion mechanism occurs when the surface temperature of the layer exceeds $0.9T_c$, where T_c is the critical temperature. Kudryashov et al. [60] reported a significant drop in reflectivity when studying the ablation of graphite by nanosecond KrF laser at intermediate laser fluences, attributing it to the phase explosion effect. In another study, Wu and Shin [61] theoretically calculated the absorption coefficient of aluminum near the critical point at a wavelength of 532 nm using the Drude model. They found that the absorption coefficient was about three orders of magnitude smaller than the value at room temperature. Moreover, the wavelength effect on the absorption coefficient of aluminum near the critical point has been demonstrated in [61,62], where the absorption coefficient is predicted to decrease with increasing the wavelength.

4. Conclusions

In this study, we have performed a comparative study on the reflection on nanosecond laser pulses with two different wavelengths (1.06 μm and 0.69 μm) in the ablation of niobium in air. Our experiments are consistent with previous results [20,21] and show that at low laser fluences, the laser wavelength effect is most noticeable, but as the laser fluence increases beyond the plasma formation threshold, the laser wavelength effect becomes insignificant and remains unchanged with further fluence increase. Further analysis of the surface temperature at the plasma formation fluence reveals that the calculated surface temperature is significantly below the melting point of the niobium sample, this suggests that micro/nano defects play an important role in the reflectivity drop due to plasmonic absorption. Taking into account the absorption of the laser light by plasma reveals that reflectivity values for both wavelengths are a little different, but these discrepancies can be neglected since the sample used by the authors in reference [51] had a purity of 99.9%, which in practical applications is very rare to find. Nano/micro defects, oxide films, and

contaminants result in a more pronounced wavelength effect on the reflectivity. Additionally, nanoscale transient ripples on the surface of the melted layer can affect reflectivity through the Fresnel angular dependence. We hold the view that the absorption of laser light by plasma is crucial in mitigating the wavelength-induced impact on the overall reflectivity in our empirical findings when $F > 10 \text{ J/cm}^2$. When the laser wavelength increases, the absorption of laser light in plasma decreases.

Author Contributions: Conceptualization, O.B. and A.F.G.; Data curation, L.d.l.C.M.; Funding acquisition, A.F.G.; Investigation, O.B. and E.M.B.; Methodology, O.B.; Project administration, O.B. and A.F.G.; Resources, L.d.l.C.M.; Writing—original draft, L.d.l.C.M.; Writing—review & editing, O.B. and E.M.B. All authors have read and agreed to the published version of the manuscript.

Funding: This research received no external funding.

Institutional Review Board Statement: The study did not require ethical approval.

Informed Consent Statement: Not applicable.

Data Availability Statement: Not applicable.

Conflicts of Interest: The authors declare no conflict of interest.

References

1. Lazarus, N.; Smith, G.L.; Dickey, M.D. Self-Folding Metal Origami. *Adv. Intell. Syst.* **2019**, *1*, 1900059. [[CrossRef](#)]
2. Ashfold, M.; Claeysens, F.; Fuge, G.; Henley, S. Pulsed Laser Ablation and Deposition of Thin Films. *Chem. Soc. Rev.* **2004**, *33*, 23–31. [[CrossRef](#)]
3. Irimiciuc, S.A.; Chertopalov, S.; Lancok, J.; Craciun, V. Langmuir Probe Technique for Plasma Characterization during Pulsed Laser Deposition Process. *Coatings* **2021**, *11*, 762. [[CrossRef](#)]
4. György, E.; Pérez, A.; Pérez Del Pino, A.; Serra, P.; Morenza, J. Influence of the ambient gas in laser structuring of the titanium surface. *Surf. Coat. Technol.* **2004**, *187*, 245–249. [[CrossRef](#)]
5. Bulgakova, N.M.; Panchenko, A.N.; Tel'minov, A.E.; Shulepov, M.A. Formation of microtower structures on nanosecond laser ablation of liquid metals. *Appl. Phys. A* **2009**, *98*, 393. [[CrossRef](#)]
6. Pedraza, A.J.; Fowlkes, J.D.; Guan, Y.F. Surface nanostructuring of silicon. *Appl. Phys. A* **2003**, *77*, 277–284. [[CrossRef](#)]
7. Wang, Z.B.; Hong, M.H.; Luk'yanchuk, B.S.; Huang, S.M.; Wang, Q.F.; Shi, L.P.; Chong, T.C. Parallel nanostructuring of GeSbTe film with particle mask. *Appl. Phys. A* **2004**, *79*, 1603–1606. [[CrossRef](#)]
8. Hendow, S.T.; Shakir, S.A. Structuring materials with nanosecond laser pulses. *Opt. Express* **2010**, *18*, 10188–10199. [[CrossRef](#)] [[PubMed](#)]
9. Visser, C.W.; Pohl, R.; Sun, C.; Römer, G.W.; Huisin't Veld, B.; Lohse, D. Toward 3D Printing of Pure Metals by Laser-Induced Forward Transfer. *Adv. Mater.* **2015**, *27*, 4087–4092. [[CrossRef](#)]
10. Zorba, V.; Boukos, N.; Zergioti, I.; Fotakis, C. Ultraviolet femtosecond, picosecond and nanosecond laser microstructuring of silicon: Structural and optical properties. *Appl. Opt.* **2008**, *47*, 1846–1850. [[CrossRef](#)]
11. Tang, G.; Hourd, A.C.; Abdolvand, A. Nanosecond pulsed laser blackening of copper. *Appl. Phys. Lett.* **2012**, *101*, 231902. [[CrossRef](#)]
12. Russo, R.E.; Mao, X.L.; Borisov, O.V.; Liu, H. Influence of wavelength on fractionation in laser ablation ICP-MS. *J. Anal. Atomic Spectrom.* **2000**, *15*, 1115–1120. [[CrossRef](#)]
13. Gottfried, J.L.; De Lucia, F.C., Jr.; Munson, C.A.; Miziolek, A.W. Laser-induced breakdown spectroscopy for detection of explosives residues: A review of recent advances, challenges, and future prospects. *Anal. Bioanal. Chem.* **2009**, *395*, 283–300. [[CrossRef](#)] [[PubMed](#)]
14. Ta, D.V.; Dunn, A.; Wasley, T.J.; Kay, R.W.; Stringer, J.; Smith, P.J.; Connaughton, C.; Shephard, J.D. Nanosecond laser textured superhydrophobic metallic surfaces and their chemical sensing applications. *Appl. Surf. Sci.* **2015**, *357*, 248–254. [[CrossRef](#)]
15. Ocaña, J.L.; Jagdheesh, R.; García-Ballesteros, J.J. Direct generation of superhydrophobic microstructures in metals by UV laser sources in the nanosecond regime. *Adv. Opt. Technol.* **2016**, *5*, 87–93. [[CrossRef](#)]
16. Cheng, J.-Y.; Yen, M.-H.; Wei, C.-W.; Chuang, Y.-C.; Young, T.-H. Crack-free direct-writing on glass using a low-power UV laser in the manufacture of a microfluidic chip. *J. Micromech. Microeng.* **2005**, *15*, 1147–1156. [[CrossRef](#)]
17. Bonch-Bruevich, A.M.; Imas, Y.A.; Romanov, G.S.; Libenson, M.N.; Mal'tsev, L.N. Effect of a laser pulse on the reflecting power of a metal. *Sov. Phys. Technol. Phys.* **1968**, *13*, 640–643.
18. Basov, N.G.; Boiko, V.A.; Krokhin, O.N.; Semenov, O.G.; Sklizkov, G.V. Reduction of reflection coefficient for intense laser radiation of solid surfaces. *Sov. Phys. Technol. Phys.* **1969**, *13*, 1581–1582.
19. Benavides, O.; de la Cruz May, L.; Flores Gil, A. A comparative study on reflection of nanosecond Nd-YAG laser pulses in ablation of metals in air and in vacuum. *Opt. Express* **2013**, *21*, 13068–13073. [[CrossRef](#)]

20. Benavides, O.; de la Cruz May, L.; Flores Gil, A.; Jimenez, L.J.A. Experimental study on reflection of high-intensity nanosecond Nd: YAG laser pulses in ablation of metals. *Opt. Lasers Eng.* **2015**, *68*, 83–86. [[CrossRef](#)]
21. Benavides, O.; de la Cruz May, L.; Mejia, E.B.; Hernandez, J.A.R.; Gil, A.F. Laser wavelength effect on nanosecond laser light reflection in ablation of metals. *Laser Phys.* **2016**, *26*, 126101. [[CrossRef](#)]
22. Nikishina, E.E.; Drobot, D.V.; Lebedeva, E.N. Niobium and tantalum: State of the world market, fields of application, and raw sources. Part I. *Rus. J. Non-Ferrous Metals* **2013**, *54*, 446–452. [[CrossRef](#)]
23. Grill, R.; Gnadenberger, A. Niobium as mint metal: Production properties processing. *Int. J. Refract. Metals Hard Mater.* **2006**, *24*, 275–282. [[CrossRef](#)]
24. Laverick, C. Niobium demand and superconductor applications: An overview. *J. Less Common Metals* **1988**, *139*, 107–122. [[CrossRef](#)]
25. Eason, R. *Pulsed Laser Deposition of Thin Films: Applications-Led Growth of Functional Materials*; John Wiley & Sons: Hoboken, NJ, USA, 2007.
26. Li, X.; Li, Y.; Zou, G.; Zhang, H.; Wang, Z. Effect of laser wavelength on ablation characteristics of copper. *J. Mater. Sci. Technol.* **2019**, *35*, 239–245.
27. Bhu-Shan, B. *Springer Handbook of Nanotechnology*; Springer: Berlin/Heidelberg, Germany, 2017.
28. L'Huillier, J.A.; Allen, C.B. Wavelength dependence of the reflectivity of aluminum and copper at normal incidence in the EUV and soft x-ray ranges. *J. Appl. Phys.* **2015**, *118*, 205301.
29. Shafeev, G.A.; Nishimura, T.; Baba, M. Effect of laser wavelength on the efficiency of copper ablation by femtosecond laser pulses. *Appl. Phys. A* **2003**, *77*, 489–492.
30. Tayyab, M.; Bhardwaj, R. Resonance-enhanced ablation of metals: Influence of laser polarization and wavelength. *Opt. Express* **2015**, *23*, 22747–22756.
31. Liu, J.; Chen, J.; Li, W.; Li, G. Effect of laser wavelength on ablation threshold and processing characteristics of nickel thin film. *Appl. Surf. Sci.* **2017**, *419*, 293–298.
32. Li, W.; Li, G.; Hu, Y.; Li, Z.; Liu, J. Effect of laser wavelength on laser-induced periodic surface structures formation on titanium thin film. *Appl. Surf. Sci.* **2019**, *478*, 119–127.
33. Zuber, M.; Baumeier, B.; Böhme, R. Influence of laser wavelength on material removal rate, roughness and recast layer thickness in micro laser engraving of tool steel. *J. Manuf. Proc.* **2020**, *59*, 14–25.
34. Benavides, O.; De La Cruz May, L.; Flores Gil, A. *Handbooks Aplicaciones Laser en la Ingeniería*. Ecorfan Editorial, December 2021, Mexico. Available online: https://www.ecorfan.org/handbooks/Handbooks_Aplicaciones_Laser_en_la_Ingenieria_TI/Handbooks_Aplicaciones_Laser_en_la_Ingenieria_TI.pdf (accessed on 26 March 2023).
35. Benavides, O.; Golikov, V.; Lebedeva, O. Reflection of high-intensity nanosecond Nd:YAG laser pulses by metals. *Appl. Phys. A* **2013**, *112*, 113–117. [[CrossRef](#)]
36. Vorobyev, A.Y.; Guo, C. Reflection of femtosecond laser light in multipulse ablation of metals. *J. Appl. Phys.* **2011**, *110*, 043102. [[CrossRef](#)]
37. Vorobyev, A.Y.; Kuzmichev, V.M.; Kokody, N.G.; Kohns, P.; Dai, J.; Guo, C. Residual thermal effects in Al following single ns- and fs-laser pulse ablation. *Appl. Phys. A* **2006**, *82*, 357–362. [[CrossRef](#)]
38. Winter, K.M.; Kalucki, J.; Koshel, D. 3-Process technologies for thermochemical surface engineering. In *Thermochemical Surface Engineering of Steels*; Mittemeijer, E.J., Somers, M.A.J., Eds.; Woodhead Publishing: Oxford, UK, 2015; pp. 141–206.
39. Libenson, M.N.; Romanov, G.S.; Imas, Y.A. Temperature dependence of the optical constants of a metal in heating by laser radiation. *Sov. Phys. -Technol. Phys.* **1969**, *13*, 925–927.
40. Ujihara, K. Reflectivity of Metals at High Temperatures. *J. Appl. Phys.* **1972**, *43*, 2376–2383. [[CrossRef](#)]
41. Ready, J.R. *Effects of High-Power Laser Radiation*; Academic Press: New York, NY, USA, 1971.
42. Anisimov, S.I.; Khokhlov, V.A. *Instabilities in Laser-Matter Interaction*. L.D. Landau Institute for Theoretical Physics; CRC Press: Boca Raton, FL, USA, 1995; ISBN 0-8493-8660-8.
43. Prokhorov, A.M.; Konov, V.I.; Ursu, I.; Mihailescu, I.N. *Laser Heating of Metals*; Adam Hilger: Bristol, UK, 1990.
44. Walters, C.T.; Barnes, R.H.; Beverly III, R.E. Initiation of laser-supported-detonation (LSD) waves. *J. Appl. Phys.* **1978**, *49*, 2937–2949. [[CrossRef](#)]
45. Vorobyev, A.Y.; Kuz'michev, V.M. Absorption of laser radiation in craters on metal targets. *Sov. J. Quantum Electr.* **1980**, *7*, 183–186. [[CrossRef](#)]
46. Tokarev, V.N.; Lunney, J.G.; Marine, W.; Sentis, M. Analytical thermal model of ultraviolet laser ablation with single-photon absorption in the plume. *J. Appl. Phys.* **1995**, *78*, 1241–1246. [[CrossRef](#)]
47. Wen, S.-B.; Mao, X.; Greif, R.; Russo, R.E. Laser ablation induced vapor plume expansion into a background gas. II. Experimental analysis. *J. Appl. Phys.* **2007**, *101*, 023115. [[CrossRef](#)]
48. Radziemski, L.J.; Cremers, D.A. *Laser-Induced Plasmas and Applications*; Marcel Dekker Inc.: New York, NY, USA, 1989.
49. Born, M.; Wolf, E. *Principles of Optics*; Pergamon Press: Oxford, UK, 1980.
50. Kirkwood, S.E.; Tsui, Y.Y.; Fedosejevs, R.; Brantov, A.V.; Bychenkov, V.Y. Experimental and theoretical study of absorption of femtosecond laser pulses in interaction with solid copper targets. *Phys. Rev. B* **2009**, *79*, 144120. [[CrossRef](#)]
51. Golovashkin, A.I.; Leksina, I.E.; Motulevich, G.P.; Shubin, A.A. The Optical Properties of Niobium. *Zh. Eksp. Teor. Fiz.* **1968**, *56*, 51–64.

52. Weaver, J.H.; Lynch, D.W.; Olson, C.G. Optical Properties of Niobium from 0.1 to 36.4 eV. *Phys. Rev. B* **1973**, *7*, 4311–4318. [[CrossRef](#)]
53. Marla, D.; Bhandarkar, U.V.; Joshi, S.S. A model of laser ablation with temperature-dependent material properties, vaporization, phase explosion and plasma shielding. *Appl. Phys. A* **2014**, *116*, 273–285. [[CrossRef](#)]
54. Kelly, R.; Miotello, A. Comments on explosive mechanisms of laser sputtering. *Appl. Surf. Sci.* **1996**, *96–98*, 205–215. [[CrossRef](#)]
55. Porneala, C.; Willis, D. Observation of nanosecond laser-induced phase explosion in aluminum. *Appl. Phys. Lett.* **2006**, *89*, 211121. [[CrossRef](#)]
56. Guillemot, F.; Prima, F.; Tokarev, V.N.; Belin, C.; Porté-Durrieu, M.C.; Gloriant, T.; Lazare, S. Single-pulse KrF laser ablation and nanopatterning in vacuum of β -titanium alloys used in biomedical applications. *Appl. Phys. A* **2004**, *79*, 811–813. [[CrossRef](#)]
57. Smith, N.V. The optical properties of liquid metals. *Adv. Phys.* **1967**, *16*, 629–636. [[CrossRef](#)]
58. Hodgson, J.N. The optical properties of liquid indium, cadmium, bismuth and antimony. *Philos. Mag J. Theor. Exp. Appl. Phys.* **1962**, *7*, 229–236. [[CrossRef](#)]
59. Abeles, F. (Ed.) *Optical Properties and Electronic Structure of Metals and Alloys*; North-Holland: Amsterdam, The Netherlands, 1966.
60. Kudryashov, S.I.; Tikhov, A.A.; Zvorykin, V.D. Near-critical nanosecond laser-induced phase explosion on graphite surface. *Appl. Phys. A* **2011**, *102*, 493–499. [[CrossRef](#)]
61. Wu, B.; Shin, Y.C. Absorption coefficient of aluminum near the critical point and the consequences on high-power nanosecond laser ablation. *Appl. Phys. Lett.* **2006**, *89*, 111902. [[CrossRef](#)]
62. Cao, Y.; Zhao, X.; Shin, Y.C. Analysis of nanosecond laser ablation of aluminum with and without phase explosion in air and water. *J. Laser Appl.* **2013**, *25*, 032002. [[CrossRef](#)]

Disclaimer/Publisher’s Note: The statements, opinions and data contained in all publications are solely those of the individual author(s) and contributor(s) and not of MDPI and/or the editor(s). MDPI and/or the editor(s) disclaim responsibility for any injury to people or property resulting from any ideas, methods, instructions or products referred to in the content.